Materials Science & Engineering A 946 (2025) 149109

Contents lists available at ScienceDirect

Materials Science & Engineering A

journal homepage: www.elsevier.com/locate/msea

Interfacial segregation of Fe and Si on TiB_2 surface and refinement of Fe-bearing intermetallic compounds and primary Si Part II Refinement of primary Fe-intermetallic compounds and primary Si through manipulating nucleation potency of TiB_2 particles

Zhongping Que [a,*], Yun Wang [a], Zhongyun Fan [a], Xiaorong Zhou [b]

[a] Brunel Centre for Advanced Solidification Technology (BCAST), Brunel University London, Uxbridge, Middlesex, UB8 3PH, UK
[b] School of Materials, University of Manchester, Manchester, M13 9PL, UK

ARTICLE INFO

Keywords:
Interfacial segregation
Compositional templating
Heterogeneous nucleation
TiB_2
Al-alloys

ABSTRACT

In Part I of this study, the interfacial segregation of Fe and Si at the Al/TiB_2 interface in an Al-3.7Ti-1.5B-1.0Fe-1.0Si master alloy was reported, with the structure and chemistry of the interfacial layers investigated using high-resolution transmission electron microscopy (HRTEM). In Part II, the TiB_2 particles, in which Fe and Si segregation had been established, were introduced into Al-Fe-Si and Al-Si alloys, respectively. The objective was to enhance heterogeneous nucleation of primary Fe-containing intermetallic compounds (Fe-IMCs) and primary Si particles in these alloys. Experimental results demonstrate that the primary β-$Al_{4.5}FeSi$ IMCs and primary Si particles were significantly refined by the inoculation of TiB_2 particles exhibiting Fe and Si segregation on their surfaces. This refinement is attributed to the high nucleation potency of the segregated TiB_2, which provides both compositional and structural templating. Well-defined orientation relationships at the Fe-IMC/(Fe, Si)TiB_2 and Si/(Fe, Si)TiB_2 interfaces were observed, offering solid evidence that both primary phases nucleate heterogeneously on the surface of segregated TiB_2 particles. These findings further validate the proposed mechanism, that both structural and compositional templating are necessary to enhance the nucleation of primary phases.

1. Introduction

A refined and uniform microstructure is usually desirable for cast metallic alloys, in order to achieve reduced casting defects and improved mechanical properties, such as strength, hardness and ductility [1–3]. Besides grain refinement of matrix, the size and morphology of secondary phases such as intermetallic compounds in an aluminium alloy play an important role in determining the mechanical properties.

In particular, aluminium alloys with high concentrations of alloying elements such as Fe and Si tend to form large primary Fe-bearing intermetallic compounds (Fe-IMCs) [4,5] or primary Si particles [6,7] during solidification. These coarse phases are associated with a higher susceptibility to casting defects, including porosity and hot tearing, and have a detrimental effect on mechanical properties. Although various studies have been conducted over the past few decades, the mechanisms governing the heterogeneous nucleation of these secondary phases remain poorly understood. Moreover, the development of effective refining techniques continues to face significant challenges.

As both an unavoidable impurity and an essential alloying element in most aluminium alloys, iron (Fe) plays a significant role in determining mechanical properties, particularly ductility [8,9]. Due to the low solid solubility of Fe in aluminium, coarse Fe-IMCs are commonly formed during the casting process. The refinement of these Fe-IMCs is critically important, especially in recycled Al alloys, where Fe and Si tend to accumulate. Since Fe-IMCs are difficult to refine in the solid state, their refinement must occur during solidification, by effectively controlling both their nucleation and growth mechanisms.

Due to structural complexity and multiple elemental compositions of Fe-rich compounds, nucleation of these phases requires not only the creation of a crystal structure but also the positioning of 2 or more types of elements in the lattice with the specified compositions. Heterogeneous nucleation of intermetallic compounds is therefore inherently more difficult and needs to overcome a much higher energy barrier than that of a pure metal or a solid solution [10]. This makes composition

* Corresponding author.
E-mail address: Zhongping.Que@brunel.ac.uk (Z. Que).

https://doi.org/10.1016/j.msea.2025.149109
Received 3 July 2025; Received in revised form 3 September 2025; Accepted 12 September 2025
Available online 12 September 2025

templating important in nucleation control in addition to structural templating [11] where lattice misfit at the interface between the nucleating solid and substrate is considered only. Fe and Si are two major impurities in Al alloys and the constitution elements of the main Fe-bearing IMCs. In Part I of the study, it has been demonstrated that Fe and Si can co-segregate at the Al/ $(1\,0\,\bar{1}\,0)$ TiB_2, leading to the formation of in-planar ordered 2-dimensional compound Al_8Fe_5 (2DC). A hypothesis is proposed in this study that this 2DC could provide both composition templating and structural templating for the heterogeneous nucleation of Fe-bearing IMCs.

Al-Si based alloys have wide applications as light weight engineering materials due to their good castability, machinability, and desirable mechanical properties [12,13]. Their high strength and wear resistance properties are mainly contributed by the primary Si particles [14,15]. However, the primary Si particles in hypereutectic Al-Si alloys are usually of large size with dendritic, platelet or polygon morphologies, which deteriorates the mechanical properties. Refinement of Si particles during the solidification is highly demanded. Over the last few decades, addition of phosphorus-containing master alloys such as Cu-P [16], Al-P [17], Al-Si-P [18], or Al-Fe-P [19], Sr-P [20], etc. has been one of the most effective ways to refine the primary silicon in the hypereutectic Al-Si alloys. The refinement of Al-Si alloys from hypoeutectic to hypereutectic alloys by addition of Al-Ti-B master alloys are extensively investigated also [21,22]. However, the usage of the master alloys as the modifier brings in various issues, such as higher modification temperature for Cu-P, increasing Fe content from the addition of Al-Fe-P master alloy. Development of effective refining ways with stable modification effects and without impurity elements is still in need. Despite being a single-element phase rather than a complex intermetallic like Fe-IMCs, Si nucleation does not require multi-element lattice positioning, and its nucleation mechanism is surely more complicated. This demands a deep understanding of its nucleation difficulty in order to effectively refine the primary Si in Al-Si based alloys.

In Part I of this study [23], have demonstrated that Fe and Si exhibit different segregation behaviour depending on atomic configuration on the prismatic and basal TiB_2 surfaces in the prepared Al-3.7Ti-1.5B-1.5Fe-1.0Si master alloy. While Si segregates on all the terminating surfaces of TiB_2, Fe segregation, combined with Si segregation, is found only on the $(1\,0\,\bar{1}\,0)$ TiB_2 surface, leading to the formation of an Al_8Fe_5 2-dimensional compound (2DC) at the Al/ $(1\,0\,\bar{1}\,0)$ TiB_2 interface. Si segregation on (0 0 0 1) TiB_2 surface resulted in partial dissolution of the pre-existing Al_3Ti 2DC, and incorporated into the Al_3Ti 2DC. The formation of Al_8Fe_5 2DC layer at Al/ $(1\,0\,\bar{1}\,0)$ TiB_2 interface and Si segregated Al/(0 0 0 1)TiB_2 interface, could potentially provide both the compositional templating and structural templating required for heterogeneous nucleation of Fe-bearing IMCs and primary Si phases, respectively. In the Part II, here we validate the hypothesis that nucleation of Fe-IMCs and Si phases can be greatly promoted through synergy of the two types of templating, eventually resulting in significant refinement of the primary IMCs and primary Si crystals in Al-14.8Si-0.7Mn-3.9Fe and Al-27Si alloy, respectively, inoculated by TiB_2 particles in Al-3.7Ti-1.5B-1.5Fe-1.0Si master alloy. Based on the experimental evidence of the achieved refinement of both the primary phases, the underlying mechanisms were proposed and extensively discussed in terms of heterogeneous nucleation of the primary phases on the modified TiB_2 particles, with the borides specifically providing both compositional and structural templating.

2. Experimental

2.1. Alloy preparation and inoculation

Al-14.8Si-0.7Mn-3.9Fe alloy was prepared by heating commercial purity Al (>99.86 %) (All compositions are in wt.% unless specified otherwise) ingot up to 750 °C, followed by addition of certain amount of Al-20 %Mn, Al-50 %Si, and Al-38 %Fe master alloys. Al-27Si alloy was similarly prepared by melting CP Al and Al-50 %Si master alloy at 870 °C. During the preparation, the alloy ingots were heated, and the melts were isothermally held in an electric resistance furnace at the target temperatures, with occasionally stirring to allow a fully dissolution of the alloying elements in the master alloys.

The prepared Al-3.7Ti-1.5B-1.5Fe-1.0Si master alloy, which contains TiB_2 particles with Fe and Si segregation on their surfaces [23], was added to the prepared Al-14.8Si-0.7Mn-3.9Fe alloy and Al-27 Si alloy with the concentration being 0.1 wt% and 0.5 wt% of the master alloy, respectively. The melts inoculated with the TiB_2 particles from the pre-prepared master alloy was stirred to ensure a complete homogeneity, with the slag on the surface being removed prior casting. The final composition of the alloy was measured by spark chemical analyses using a 'foundry master' instrument. Both the melts were then divided into two equal amounts for the casting with and without grain refiner. 1000 ppm (0.1 %) and 5000 ppm (0.5 %) of Al-3.7Ti-1.5B-1.5Fe-1.0Si master alloy were added into the Al-14.8Si-0.7Mn-3.9Fe alloy and Al-27Si alloy melts, respectively, regarding to the difference on the volume fraction of the primary phases. After completely stirring, the melts were cast at 50 °C above the liquidus into a pre-heated TP-1 mould at 380 °C. The mould was immediately cooled by a water spray with a controlled water flow rate of 3.8 L/min [24]. It is important to note that the melt was casted within 20 min after the addition of grain refiner in case the interfacial segregation of added TiB_2 were affected in the melt. The primary Fe-rich intermetallic compound and Si particles that solidified in the remaining Al-14.8Si-0.7Mn-3.9Fe alloy and Al-27Si alloy melts, after the addition of grain refiner, were collected through sedimentation to facilitate TEM examinations.

2.2. Characterization

Morphology and size distribution of the synthesized boride particles were examined by scanning electron microscopy (SEM) using a Zeiss Supera 35 SEM instrument operated at an accelerating voltage of 5–20 kV. To investigate the 3-dimensional (3D) morphology of the TiB_2 particles, the samples were deep-etched using an aqueous solution containing 15 vol% HCl by dissolving the Al matrix, followed by cleaning in an ethanol bath.

The samples for transmission electron microscopy (TEM) examinations were prepared from 3 mm diameter discs. The discs were ground to a thickness of less than 50 μm before further thinning by Ar ion beam milling using a Gatan precision ion polishing system (PIPS) under a voltage of 1.0–5.0 kV and an incident beam angle of 3–5°.

The TP-1 cast samples were sectioned in cross section at 38 mm height from the bottom of the cast ingot where had experienced a cooling rate of 3.5 K/s [24]. Metallographic specimens were made by the standard procedures. A Zeiss optical microscope fitted with the Axio Vision 4.3 image analysis system was used for the assessment of the primary β-$Al_{4.5}FeSi$ and primary Si particles. Mean linear intercept technique was used to quantify the particle size with measurement of at least 100 particles. Looking like needles in 2D section, the size of the thin plate-like Fe-rich intermetallic compound was measured by its length. Similarly, size of the primary Si, which is irregular shaped, was quantified according to its longest length in the cross section. The number density measurement of TiB_2 is calculated based on the composition of master alloys and average particle size and size distribution. The number density measurement of primary β-$Al_{4.5}FeSi$ and Si are mainly calculated according to the particle size and size distribution and the volume of materials.

To reveal interfacial segregation of alloy elements on the TiB_2 particles, atomic resolution STEM with Z-contrast high-angle annular dark filed (HAADF) imaging was carried out on an aberration (Cs)-corrected FEI Titan 80–200 instrument equipped with Super-X energy dispersive x-ray spectroscopy (Super-X EDS) system, operated with an accelerating voltage of 200 kV.

3. Results

3.1. Nature of borides with Fe and Si interfacial segregation

Fig. 1 shows the morphology of the TiB_2 particles collected from the Al-14.8Si-0.7Mn-3.9Fe alloy after addition of 0.1 wt% of Al-3.7Ti-1.5B-1.5Fe-1.0Si master alloy and segmented at the bottom of the crucible. Statistical quantification indicates that the majority TiB_2 particles are 1–3 μm in size, which are same as that in the master alloy as reported in Part 1 [23], demonstrating that the TiB_2 does not show any change in their size after the addition to the alloy melt.

Segregation of Fe and Si was repeatedly observed at the interfaces of the Al/TiB_2 by STEM and EDS mapping, as shown in Fig. 2. Si segregation (Fig. 2d) covers both the $(0\,0\,0\,1)$ and $[1\,0\,\bar{1}\,0]$ surface of the TiB_2, while Fe segregation was detected only at Al/ $(1\,0\,\bar{1}\,0)$ TiB_2 interfaces where it apparently co-segregated with Si. More details about the interfacial segregation and the formation of the 2-dimensional compounds (2DC) has been present in Part I [23]. It has been concluded that Si and Fe interfacial segregation on TiB_2 particles resulted in the formation of Al_8Fe_5 2DC at the Al/ $(1\,0\,\bar{1}\,0)$ TiB_2 interface and modification of the previously existed Al_3Ti 2DC at the Al/ $(0\,0\,0\,1)$ TiB_2 interface.

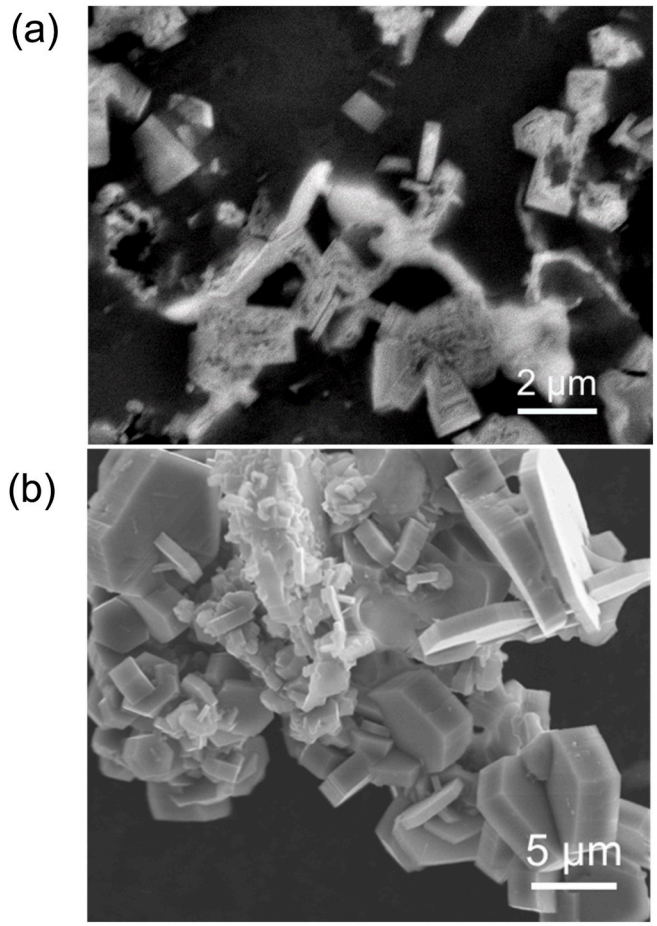

Fig. 1. SEM images showing (a) the 2-dimensional (2D) of the TiB_2 particles in Al-Ti-B-Fe-Si master alloy, and (b) 3D morphology of the collected TiB_2 particles from the Al-14.8Si-0.7Mn-3.9Fe alloy after addition of Al-3.7Ti-1.5B-1.5Fe-1.0Si master alloy and segmented at the bottom of the crucible.

3.2. Refinement of primary β-$Al_{4.5}$FeSi in Al-14.8Si-0.7Mn-3.9Fe alloy

The microstructure of Al-14.8Si-0.7Mn-3.9Fe alloy solidified at 3.5 K/s without and with the addition of 1000 ppm (0.1 %) Al-3.7Ti-1.5B-1.5Fe-1.0Si master alloy was shown in Fig. 3, where a significant refinement is seen for the needle/plate-like particles in the inoculated alloys (Fig. 3a and b). High density of porosity was observed in the Al-14.8Si-0.7Mn-3.9Fe alloy without the addition of the master alloy, as shown in Fig. 3a, due to the formation of large sized Fe-rich intermetallic compound (IMC). The casting defects were significantly reduced after the refinement of these Fe-IMCs, as shown in Fig. 3b. The high magnification microstructure of these two samples without and with grain refiner were presented in Fig. 3c and d, indicating the plate-like morphology of these primary Fe-IMC particles. This indicates that the refinement of these Fe-IMCs is mainly decrease in the length of these plates. These particles were identified as β-$Al_{4.5}$FeSi by SEM-EDS and TEM analysis (the evidence is to be given in next section). With the addition of the Al-3.7Ti-1.5B-1.5Fe-1.0Si master alloy, the average length of the IMC particles decreased from 1178 ± 135 μm (Fig. 5a) to 425 ± 61 μm (Fig. 5b).

The 3-dimensional (3D) morphology of the as-cast microstructure of the TiB_2 inoculated alloy is presented in Fig. 4. Fig. 4a shows that the needle-like (Fig. 3) particles in 2D are actually plate-like in 3D, and they have a composition of 15.7 ± 0.3 at.% Fe, 16.3 ± 0.1 at.% Si and 1.63 ± 0.03 at.% Mn, identified by SEM/EDS. TiB_2 particles are readily observed to be associated with the IMC particles typically at the grain boundaries, believing to be rejected to the solid/liquid front during solidification. Some TiB_2 particles imbedded in the primary β-$Al_{4.5}$FeSi can also be observed from Fig. 4b. However, due to the agglomeration of the TiB_2 particles, the observed TiB_2 particles that are engulfed in the Fe-IMCs are always present in clusters.

3.3. Interface between β-$Al_{4.5}$FeSi and TiB_2(Fe, Si)

The primary Fe-intermetallic β-$Al_{4.5}$FeSi particles were collected by sedimentation to facilitate TEM/STEM examinations to verify heterogeneous nucleation of β-$Al_{4.5}$FeSi on these modified TiB_2 particles. Direct evidence for nucleation of the β-$Al_{4.5}$FeSi particles was obtained, as shown in Figs. 5 and 6.

The bright field TEM image in Fig. 5a shows that a TiB_2 particle is imbedded in an Fe-bearing particle. This Fe-bearing IMCs was identified as β-$Al_{4.5}$FeSi with monoclinic crystal structure by TEM-EDS analysis and the selected area electron diffraction (SAED) patterns along different zone directions. More than one TiB_2 particle can be observed that engulfed in the β-$Al_{4.5}$FeSi particle (A and B). However, only one of the TiB_2 particles (particle B) have a defined orientation relationship (OR) with the Fe-bearing intermetallic particles. The SAED pattern with its index in Fig. 5b is from [1 1 0] direction of β-$Al_{4.5}$FeSi. Fig. 5c is the indexed SAED pattern taken from TiB_2 particles viewed along $[1\,1\,\bar{2}\,0]$ zone direction. The zone directions of [1 1 0] β-$Al_{4.5}$FeSi and $[1\,1\,\bar{2}\,0]$ of TiB_2 are not exactly parallel to each other but with small angle as 1.5°. Therefore, two sets of SAED pattern as shown in Fig. 5d were acquired in between these two sets of zone directions, encompassing the adjacent β-$Al_{4.5}$FeSi and TiB_2.

The interface between TiB_2 particle and β-$Al_{4.5}$FeSi phase was investigated at high magnifications with HRTEM, as shown by the atomic resolution images in Fig. 6. Fig. 6b and c are the FFT patterns of the β-$Al_{4.5}$FeSi in its [1 1 0] direction and TiB_2 in its $[1\,1\,\bar{2}\,0]$ direction with 1.5° deviation. According to the indexed patterns, there also exists an angle of 4° between the low indexed plane of β-$Al_{4.5}$FeSi and TiB_2 at the observed interface (Fig. 6a).

The above results from Figs. 5 and 6 reveal a specific orientation

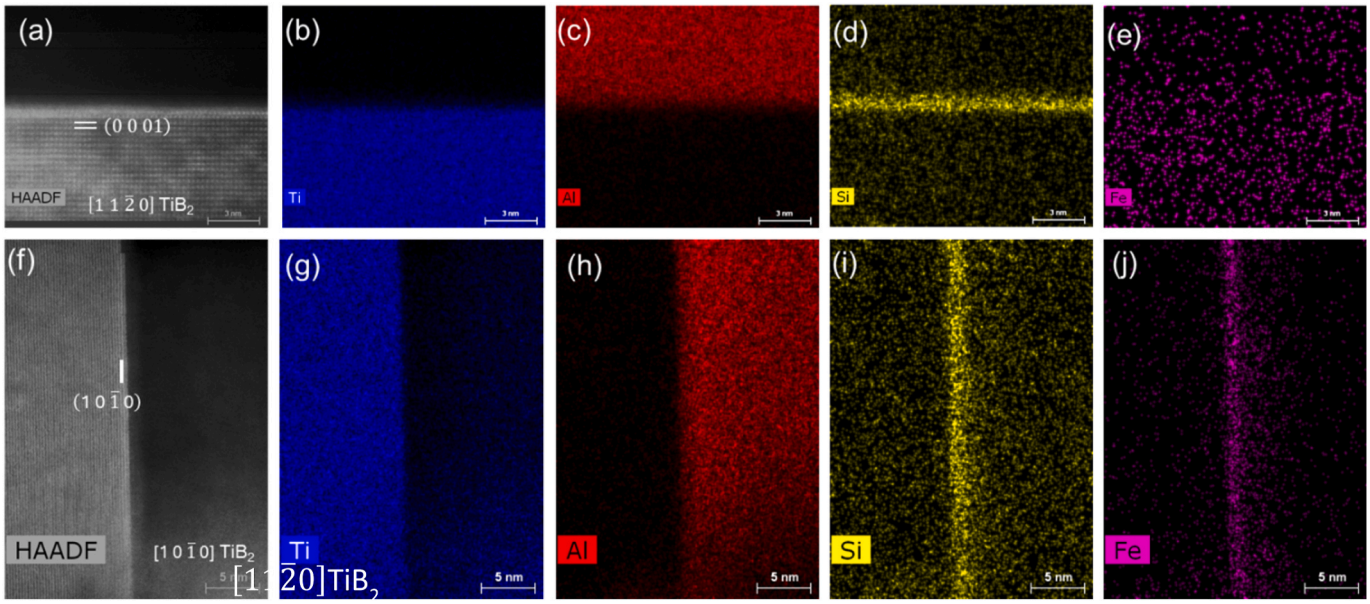

Fig. 2. STEM-EDS mapping at (a–e) Al/ $(0\ 0\ 0\ 1)$ TiB_2 interface in master alloy, with (a) high angle annular dark field (HAADF) STEM image (Z-contrast of TiB_2 particles when the incident electron beam parallels to $[1\ 1\ \bar{2}\ 0]$ direction, (b) Ti (blue), (c) Al (red), (d) Si (yellow) and (e) Fe (purple) showing the Si segregation; (f–j) Al/ $(1\ 0\ \bar{1}\ 0)$ TiB_2 interface, with (f) high angle annular dark field (HAADF) STEM image of TiB_2 particles when the incident electron beam parallels to $[1\ 0\ \bar{1}\ 0]$ direction, (g) Ti (blue), (h) Al (red), (i) Si (yellow) and (j) Fe (purple) showing the Si and Fe co-segregation at $(1\ 0\ \bar{1}\ 0)$ plane of TiB_2. (For interpretation of the references to colour in this figure legend, the reader is referred to the Web version of this article.)

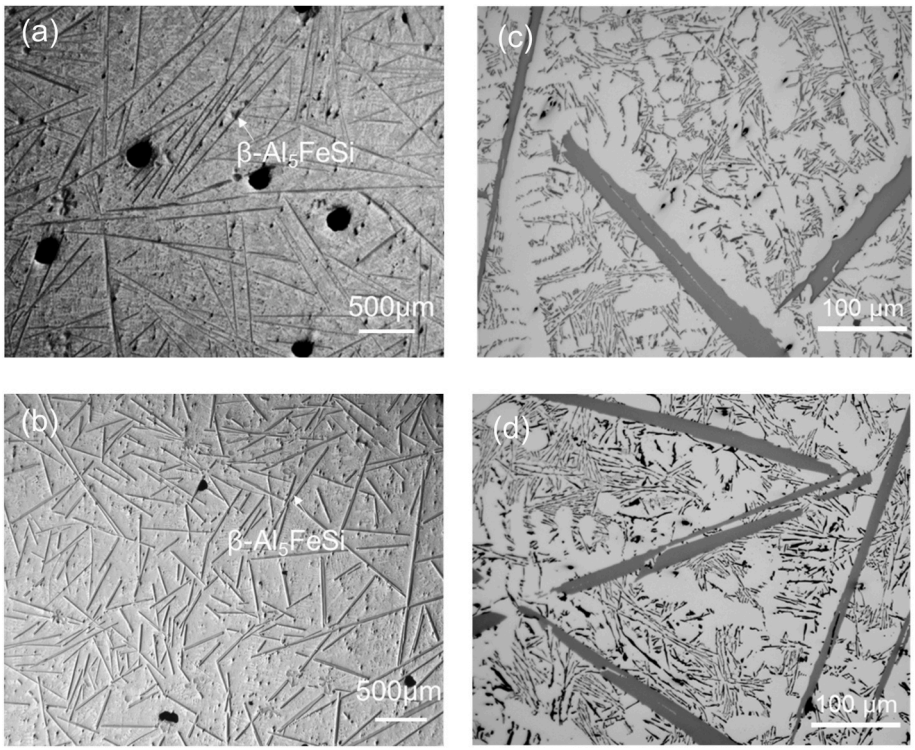

Fig. 3. Optical microstructure of as-cast Al-14.8Si-0.7Mn-3.9Fe alloy with pouring temperature of 720 °C and solidified at 3.5K/s cooling rate: (a, c) before and (b, d) after the addition of 1000 ppm Al-3.7Ti-1.5B-1.5Fe-1.0Si master alloy containing the modified TiB_2 particles with interfacial segregation of Fe and Si.

relationship (OR) between the TiB_2 particle and the β-Al_5FeSi:

$$(0\,0\,2)\beta - Al_{4.5}FeSi\,//\,4^{\circ}\,(0\,0\,0\,1)\,TiB_2, [1\,1\,0]\,\beta - Al_{4.5}FeSi\,//\,1.5^{\circ}\,[1\,1\,\bar{2}\,0]\,TiB_2 \quad \text{(OR1)}$$

By transformation of the lattices, this OR1 is found to be equivalent to the following OR2 which will have a smaller angle of 1.5° between the low indexed planes of $(\bar{2}\,2\,0)$ β-$Al_{4.5}FeSi$ and $(1\,0\,\bar{1}\,0)$ TiB_2. The investigation of the ORs between solid β-$Al_{4.5}FeSi$ and nucleation particles aims to identify the surface where actual nucleation occurs.

$$(\bar{2}\,2\,0)\beta - Al_{4.5}FeSi\,//\,1.5^{\circ}\,(1\,0\,\bar{1}\,0)\,TiB_2, [1\,1\,0]\,\beta - Al_{4.5}FeSi\,//\,1.5^{\circ}\,[1\,1\,\bar{2}\,0]\,TiB_2 \quad \text{(OR2)}$$

3.4. Refinement of primary Si in a hypereutectic Al-27Si alloy

Fig. 7 shows the as-cast microstructure of Al-27Si alloy without (Fig. 7a) and with (Fig. 7b) the addition of 0.5 wt% of Al-3.7Ti-1.5B-1.5Fe-1.0Si master alloy. It is clearly seen that, without the addition, the primary Si phase is large in size and with a dendritic morphology. Large sized porosities were also observed to be associated with these primary Si particles. With the addition of the master alloy, the primary Si particles were greatly refined, with the morphology changing from dendritic to compact. At the same time, little porosity is observed in the sample inoculated with the master alloy.

Statistical measurement of size distribution of the primary Si particles was shown in Fig. 7c. Without the addition of the master alloy, the size of the primary Si particles is in the range of 150–900 μm and an average of 461 ± 51 μm, compared to the range of 5–80 μm and average of 39 ± 5.5 μm with the addition. Expectedly, the measured number density of the primary Si particles significantly increases from 911/m^3 and 1.49 × 10^6/m^3.

The refinement of the primary Si achieved with the addition of the master alloy is comparable to that obtained by adding phosphorus in hypereutectic Al-50 Si alloy at a very large overheating where the primary Si phase was usually coarser than 30 μm in size [25,26]. Given the multiple disadvantages associated with the phosphorus addition, such as embrittlement, increased casting defects, and reduced ductility, the incorporation of TiB_2 in this study is far more desirable.

3.5. Interface between primary Si and TiB_2(Fe, Si)

Heterogeneous nucleation of the primary Si in the Al-27Si alloy on the modified TiB_2 particles is verified by direct experimental evidence, as shown in Figs. 8–10. Fig. 8a shows the interface between TiB_2 and Si phase. Fig. 8b is the SAED pattern taken from the local area across the TiB_2/Si interface when the incident electron beam is parallel to [1 1 0] of Si, with the SAED pattern being indexed in Fig. 8c. Careful analysis reveals a small deviation between [110] Si and $[1\,1\,\bar{2}\,0]$ TiB_2, with the deviation angle being measured as 2.6° by tilting of the TEM sample during the examination.

Fig. 9a is the HRTEM image showing the interface between the $(0\,0\,2)$ Si (upper part) and the $(0\,0\,0\,1)$ TiB_2 (lower part). It shows that the low indexed planes of $(0\,0\,2)$ Si is not perfectly parallel to $(0\,0\,0\,1)$ basal planes of TiB_2 with 5° deviation between them. The corresponding FFT patterns of Si and TiB_2 were shown in Fig. 9b and c, respectively. The corresponding indexed FFT patterns of Si and TiB_2 were shown in Fig. 9d and e.

The experimental observation indicates the specific orientation relationship (OR) between the TiB_2 particle and the Si shown as below:

$$(0\,0\,2)\,Si\,//\,5^{\circ}\,(0\,0\,0\,1)\,TiB_2, \text{and}\,[1\,1\,0]Si\,//\,2.6^{\circ}[1\,1\,\bar{2}\,0]\,TiB_2 \quad \text{(OR3)}$$

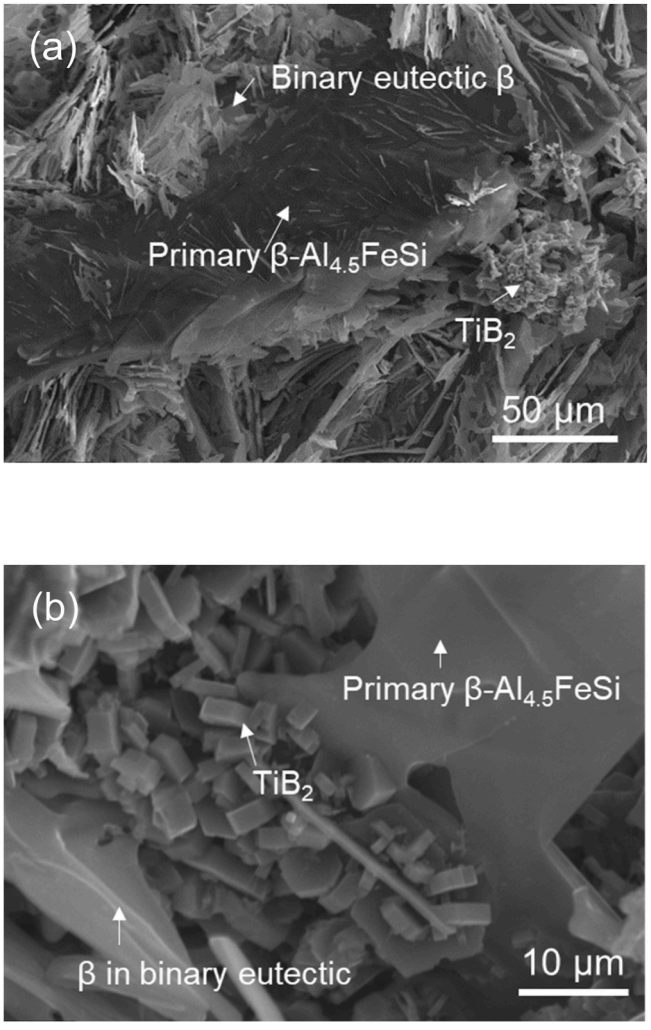

Fig. 4. SEM images showing the 3-dimensional (3D) morphology of the as-cast microstructure of Al-14.8Si-0.7Mn-3.9Fe alloy with pouring temperature of 720 °C and solidified at 3.5K/s cooling rate: (a) the plat-like primary β-$Al_{4.5}FeSi$ nucleating the binary β-$Al_{4.5}FeSi$, and (b) TiB_2 particles imbedded in the primary β-$Al_{4.5}FeSi$.

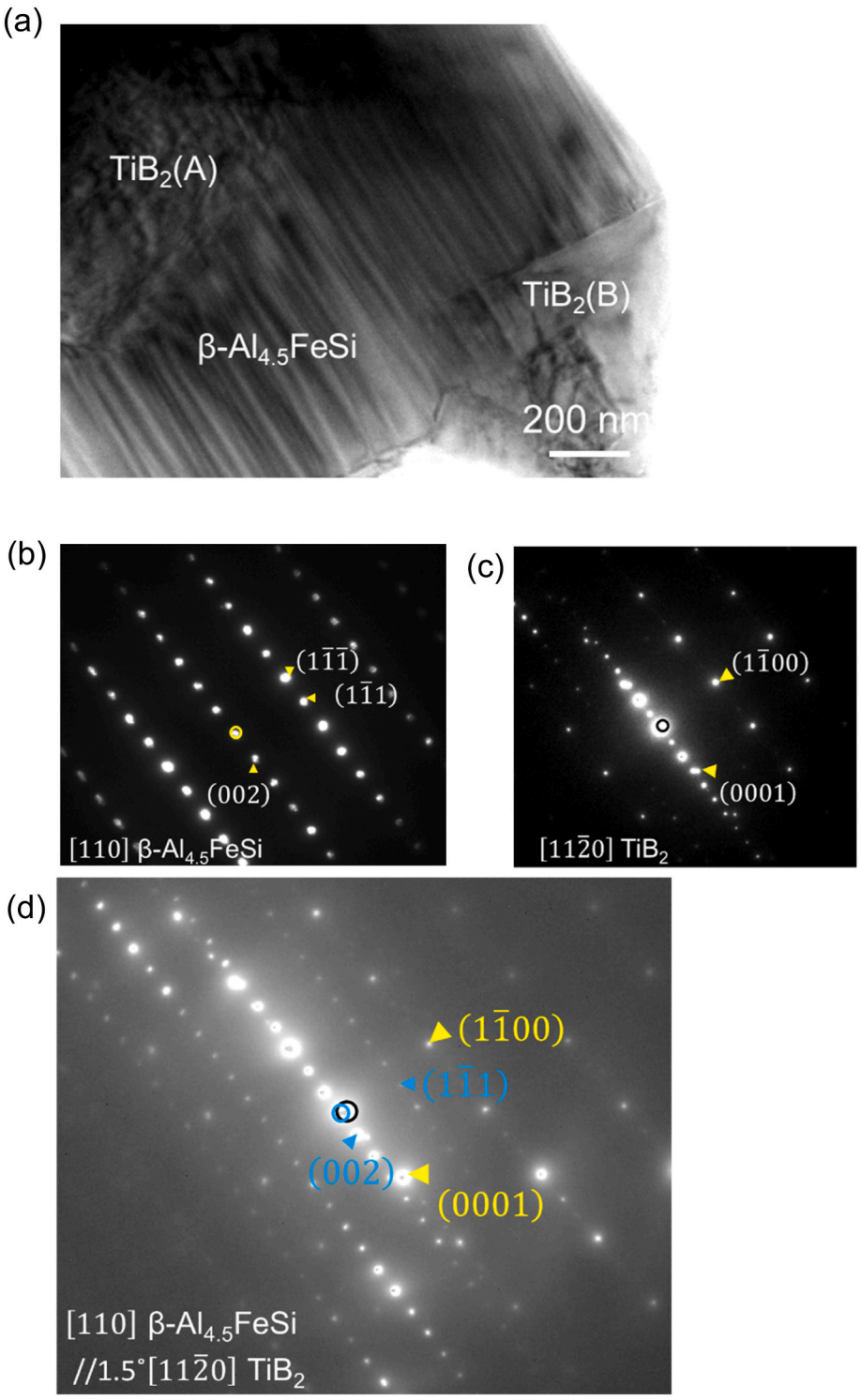

Fig. 5. (a) TEM bright field image showing a Fe and Si modified TiB_2 particle imbedded in a β-$Al_{4.5}FeSi$ intermetallic compound, (b) and (c) indexed selected area electron diffraction patterns taken from the TiB_2 particle and the intermetallic phase in the [11$\bar{2}$0] and [110] direction, respectively, and (d) indexed SAED patterns taken from both the β-$Al_{4.5}FeSi$ and TiB_2 particle.

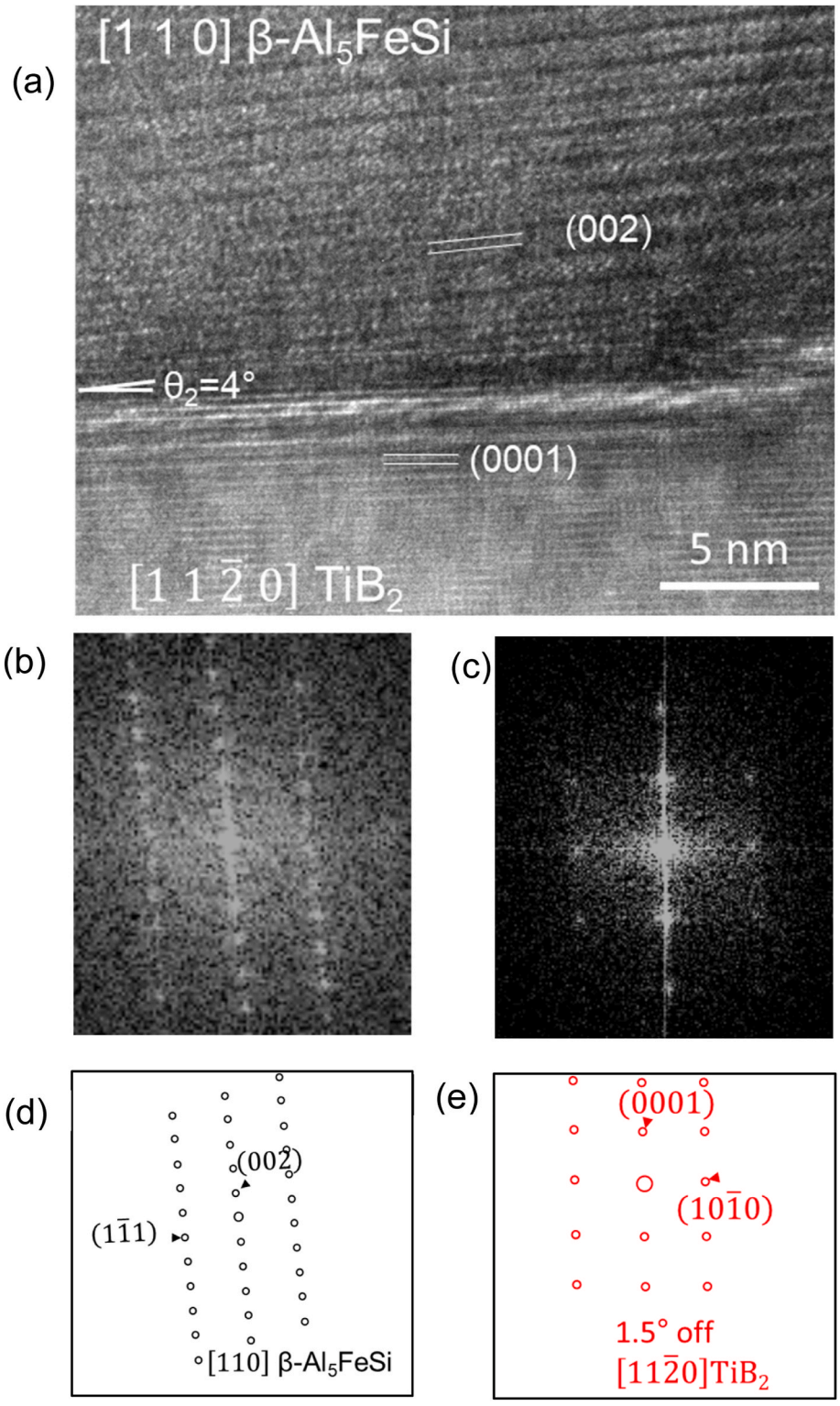

Fig. 6. (a) High resolution TEM image showing the interface between TiB_2 particle and β-Al_5FeSi phase with TiB_2 and β-Al_5FeSi being viewed along [110] and [11$\bar{2}$0] (1.5° deviation), respectively; (b) and (c) are Fast Fourier transformation (FFT) patterns for TiB_2 and β-Al_5FeSi, respectively, (d) and (e) are the schematic representation of the indexed FFT patterns of (b) and (c).

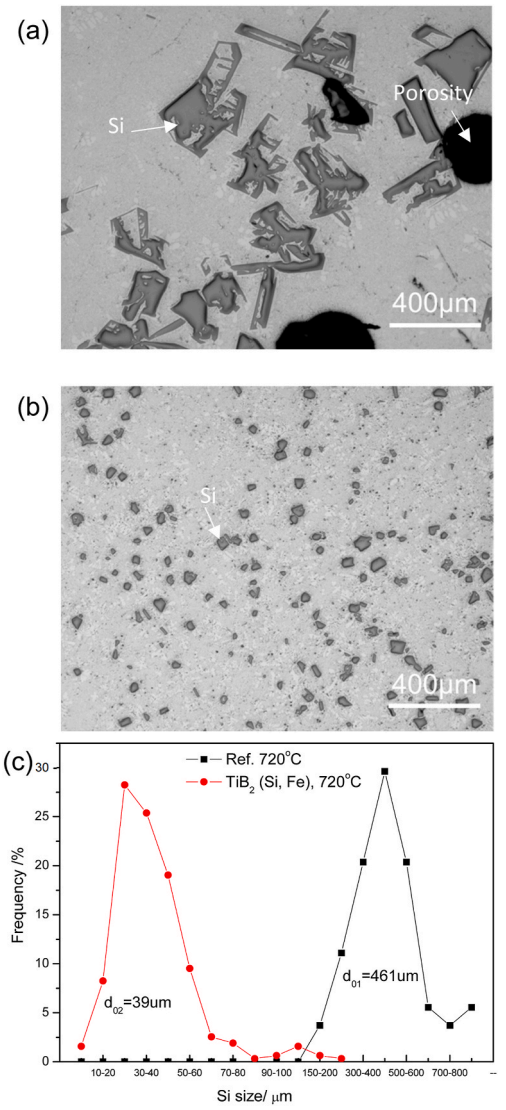

Fig. 7. Optical microstructure of Al-27Si alloy cast at 850 °C and solidified at a cooling rate of 3.5K/s: (a) before and (b) after the addition of 5000 ppm Al-3.8Ti-1.5B-1.5Fe-1.0Si master alloy containing the TiB_2 particles with interfacial segregation of Fe and Si; and (c) size distribution of the primary Si before and after grain refiner addition.

In fact, OR3 is equivalent to the following OR3a, where crystal planes $(1\,\bar{1}\,13)$ Si and $(0\,0\,0\,1)$ TiB_2 are perfectly paralleled.

$$(1\,\bar{1}\,13)\,\mathrm{Si}\ //\ (0\,0\,0\,1)\,\mathrm{TiB_2}, \text{and } [1\,1\,0]\mathrm{Si}\ //\ 2.6^{\circ}[1\,1\,\bar{2}\,0]\,\mathrm{TiB_2} \quad \text{(OR3a)}$$

Fig. 10a is HRTEM image showing the interface between the $(2\,2\,0)$ Si (upper part) and the $(1\,0\,\bar{1}\,0)$ TiB_2 (lower part). The FFT patterns of Si and TiB_2 are shown in Fig. 10b and c, respectively and their corresponding indexed FFT patterns were in Fig. 10d and e. There is 6° deviation between $(2\,2\,0)$ Si and $(1\,0\,\bar{1}\,0)$ TiB_2. The experimental observation indicates the specific orientation relationship (OR) between the TiB_2 particle and the Si shown as below, which is equivalent to OR 3:

$$(2\,\bar{2}\,0)\,\mathrm{Si}\ //\ 6^{\circ}\,(1\,0\,\bar{1}\,0)\,\mathrm{TiB_2}, \text{and } [1\,1\,0]\mathrm{Si}\ //\ 2.6^{\circ}[1\,1\,\bar{2}\,0]\,\mathrm{TiB_2} \quad \text{(OR4)}$$

Both OR3 and OR4 involve an angle between the TiB_2 surface and the nucleated Si, indicating a slightly lower potency for heterogeneous nucleation on these TiB_2 surfaces. Therefore, the competition for the heterogeneous nucleation across different substrates surfaces, as well as the roles of structural and compositional templating, will be discussed to explain the significant refinement results shown in Fig. 7. The detailed mechanism of refinement will be addressed in 4.3.

4. Discussion

4.1. Compositional and structural templating for heterogeneous nucleation of β-$Al_{4.5}$FeSi

It was reported that heterogeneous nucleation of intermetallic compounds (IMCs) is more difficult than that of a pure metal. It requires not only the creation of a crystal structure but also the positioning of 2 or more types of elements in the lattice with specified compositions. Apart from structure templating [27] for heterogeneous nucleation, another important factor is composition templating [11]. Compositional templating is a concept that by segregation the constituted alloying elements at the nucleation substrates to enhance the heterogeneous nucleation of the intermetallic compounds. The role of compositional templating for the heterogeneous nucleation of Fe-IMCs has been validated in our previous publication [11]. It is shown that Fe and Si co-segregation at the Al/$(1\,0\,\bar{1}\,0)$ AlB_2 provided both the constituted alloying element Fe and the structural templating for the heterogeneous nucleation of the α-Al_{15}(Fe, Mn)$_3Si_2$. In this study, it is proposed that once beneficial structural and compositional templating can be achieved, the type of original particles becomes less important [28]. What matter is whether the particles can provide the necessary templating to enhance the heterogenous nucleation. The experimental results in this study demonstrated that Fe and Si co-segregated on the Al/$(1\,0\,\bar{1}\,0)$ TiB_2, significantly refined the primary β-$Al_{4.5}$FeSi, which potentially validated this propose.

The modified TiB_2 studied in this work exhibits two types of interfacial segregation: co-segregation of Fe and Si at the Al/$(1\,0\,\bar{1}\,0)$ TiB_2 with Al_8Fe_5 2DC, and Si segregation alone, accompanied by modification, at the Al_3Ti 2DC/$(0\,0\,0\,1)$ TiB_2. Therefore, the specific surface of TiB_2 that facilitates the heterogeneous nucleation of β-$Al_{4.5}$FeSi needs to be discussed.

At the Al/ $(1\,0\,\bar{1}\,0)$ TiB_2 interface, Fe and Si are continuously segregated on the surface and altered the interfacial atomic arrangement including compositional and structural templating with Al_8Fe_5 2DC. The 2DC formed on TiB_2 particle replaced the original TiB_2 surface, therefore potentially changes the nucleation potency by providing the different atomic arrangement on the nucleation substrate.

Therefore, heterogeneous nucleation of β-$Al_{4.5}$FeSi occurs in only two cases: at the Al_8Fe_5 2DC/ $(1\,0\,\bar{1}\,0)$ TiB_2 or the Si modified Al_3Ti 2DC/$(0\,0\,0\,1)$ TiB_2 interface. Here, the nucleation interface between the solid and the nuclei needs to be transitioned from Al_8Fe_5 2DC/TiB_2 to β-$Al_{4.5}$FeSi/Al_8Fe_5 2DC. Therefore, two pair of new ORs (OR5 and OR6) can be generated and showed as below.

$$(\bar{2}\,2\,0)\beta-\mathrm{Al_{4.5}FeSi}\ //\ 1.5^{\circ}\ (0\,0\,1)\,\mathrm{Al_8Fe_5\ 2DC}, [1\,1\,0]\ \beta-\mathrm{Al_{4.5}FeSi}\ //\ 1.5^{\circ}\ [1\,0\,0]\,\mathrm{Al_8Fe_5\ 2DC} \quad \text{(OR5)}$$

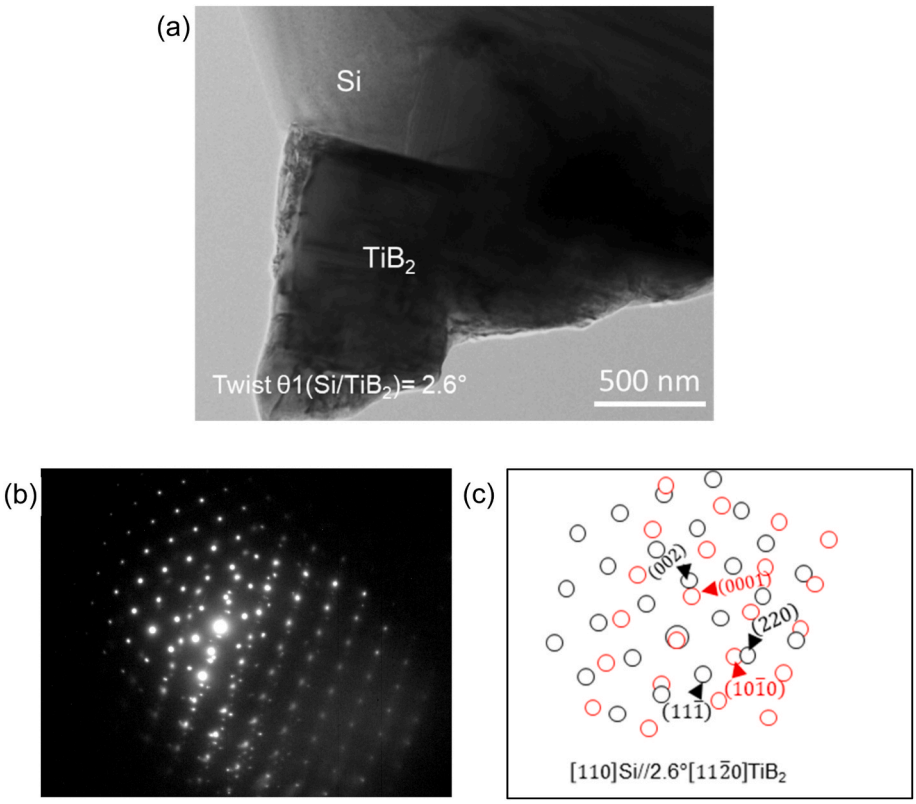

Fig. 8. (a) TEM bright field image of Si/TiB_2 interface, (b) the corresponding selected area electron diffraction (SAED) pattern taken from the TiB_2 particles and the adjacent Si phase, (c) the indexed pattern schematic of (b). The angle between the two zone directions of TiB_2 and Si was measured as 2.6°. In other words, the direction of Si perfectly parallel to [11$\bar{2}$0] TiB_2 direction is a high index direction.

and

concentration of Fe in the segregated Al_8Fe_5 2DC is higher than that in the solid β-$Al_{4.5}$FeSi phase. Furthermore, the lattice mismatch between the Al_8Fe_5 2DC and the β-$Al_{4.5}$FeSi phase is significantly reduced,

$$(0\,0\,2)\beta-Al_{4.5}FeSi\,//\,4^{\circ}\,(1\,1\,2)\,\text{Si incorporated}\,Al_3Ti\,\text{2DC},[1\,1\,0]\,\beta-Al_{4.5}FeSi\,//\,1.5^{\circ}\,[\bar{2}\,0\,1]\,\text{Si incorporated}\,Al_3Ti\,\text{2DC} \quad \text{(OR6)}$$

Indicating the potency of structural templating for heterogeneous nucleation, the lattice misfits between solid (β-$Al_{4.5}$FeSi) and nucleation substrates are calculated according to the epitaxial model for heterogeneous nucleation [27] where misfit f was defined as $(d_S - d_N)/d_S$ with S and N representing solid and nucleation substrate, respectively. Table 2 gives the calculated mismatches between the solid β-$Al_{4.5}$FeSi and the modified TiB_2 particles on both the terminated (0 0 0 1) and (1 0 $\bar{1}$ 0) planes in this study, in comparison with those on the surface of assumed "clean" (no segregation) TiB_2. Here, the calculated misfit is based on the d-spacing across the closed-packed planes of matching crystals according to the specific ORs.

It is seen from Table 2 that, firstly, (1 0 $\bar{1}$ 0) TiB_2 surface with and without interfacial segregation 2DC have smaller misfits than (0 0 0 1) TiB_2 interface for the nucleation of β-$Al_{4.5}$FeSi indicating that heterogenous nucleation more likely happens at (1 0 $\bar{1}$ 0) TiB_2 surface rather than at (0 0 0 1)TiB_2 surface. Secondary, the misfit between β-$Al_{4.5}$FeSi and TiB_2 with interfacial segregation (Al_8Fe_5 2DC) is much smaller than all the other possibilities, indicating a good structural templating. In previous studies, clean TiB_2 particles or Al-5Ti-1B grain refiner [29] has also been shown to have little refining effect on Fe-IMCs. Another important factor is composition templating. As shown in Fig. 11, the

approximately 3 %, along the Fe-enriched direction of the β-$Al_{4.5}$FeSi, suggesting a favourable orientation relationship that facilitates the templated growth.

The total number density of TiB_2 particles in the diameter range 0.2–6.0 μm in the synthesized Al-3.7Ti-1.5B-1.5Fe-1.0Si master alloy is calculated (from the volume fraction of TiB_2 and the Ti containing) to be 6.7×10^{13}/kg or $2.43 \times 10^{10}/m^3$. 0.1 % addition of such master alloy would provide a number density of TiB_2 particles about 6.7×10^{10}/kg or $2.43 \times 10^{7}/m^3$ which are available for nucleation of β-$Al_{4.5}$FeSi. With addition of 0.1 % Al-3.7Ti-1.5B-1.5Fe-1.0Si master alloy, the number density of resulted β-$Al_{4.5}$FeSi in the Al-14.8Si-0.7Mn-3.9Fe alloy was measured as $5.12 \times 10^{4}/m^3$. It demonstrated the addition of the TiB_2 particles is sufficient for nucleation of the primary β-$Al_{4.5}$FeSi. The nucleation rate calculated based on the TiB_2 particles and nucleated β-$Al_{4.5}$FeSi is 0.2 % which is at the lower range of the nucleation rate of α-Al by adding grain refiner (0.2–1 %) [30]. This also indicated the nucleation difficulty of the Fe-IMCs although with grain refinement.

4.2. *Nucleation difficulty of Si*

Nucleation of α-Al and Si involves only a single element. Aluminium and silicon are neighbours in the periodic table. Both Al [31] and Si [32] have face-centred cubic (FCC) lattices. However, nucleation of Si is

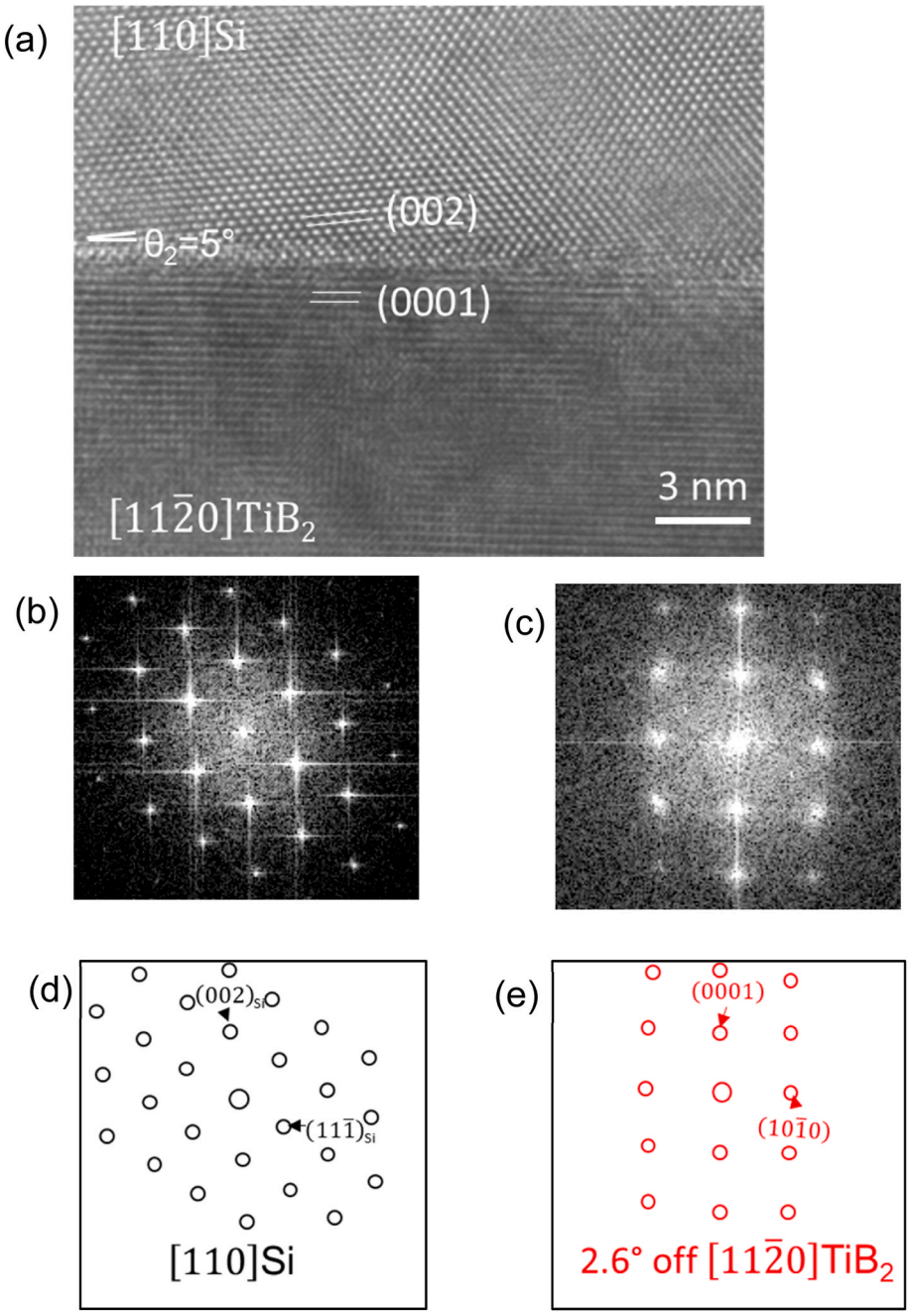

Fig. 9. (a) High resolution TEM image showing the interface between TiB_2 particle and Si phase with TiB_2 and Si being viewed along [11$\bar{2}$0] (2.6° deviation) and [110], respectively; (b) and (c) are Fast Fourier transformation (FFT) patterns for TiB_2 and Si, respectively, (d) and (e) are the schematic representation of the indexed FFT patterns of (b) and (c). These results suggest the following defined orientation relationship (OR) between TiB_2 and Si: (0001) TiB_2// (1$\bar{1}$13) Si or (0001) TiB_2//5° (002) Si and 2.6° [11$\bar{2}$0] TiB_2//[110]Si.

much more difficult and requires a nucleation undercooling as large as tens of Kelvin with the addition of P [33], compared to the value of smaller than 2 K for α-Al [33,34]. The very different heterogeneous nucleation behaviour between the silicon and aluminium could be due to the combination of energy barriers, impurity solubility, diffusion rate and surface energy factors.

The energy barrier for nucleation of silicon is higher than that of aluminium due to the crystal structure difference between diamond cubic of Si and face centred cubic of aluminium. Additionally, aluminium is a typical free-electron type metal with a densely packed stacking and each atom has twelve nearest neighbours [35]. Whereas silicon is a typical covalent solid and has the diamond-type structure, in which each Si is tetragonally coordinated with a short Si-Si bond-length of 2.35 Å, satisfying the sp^3 hybrid bonding [36]. Another difference is their electronegativity values: 1.61 Pauling unit for aluminium and 1.90 for silicon. Such notable electronegativity difference also means charge transfer ability between aluminium and silicon from the other atoms. During the solidification process of Al-alloys, once the driving force (nucleation undercooling) achieved, there will not be any energy barrier to hinder the heterogeneous nucleation of α-Al on a substrate. Therefore, the nucleation undercooling of α-Al is small. However, the coulomb interactions induce energy barriers preventing Si ions approach to each other. Correspondingly, nucleation of elemental Si requires high activation energy. Therefore, the pre-templated composition, Si, becomes

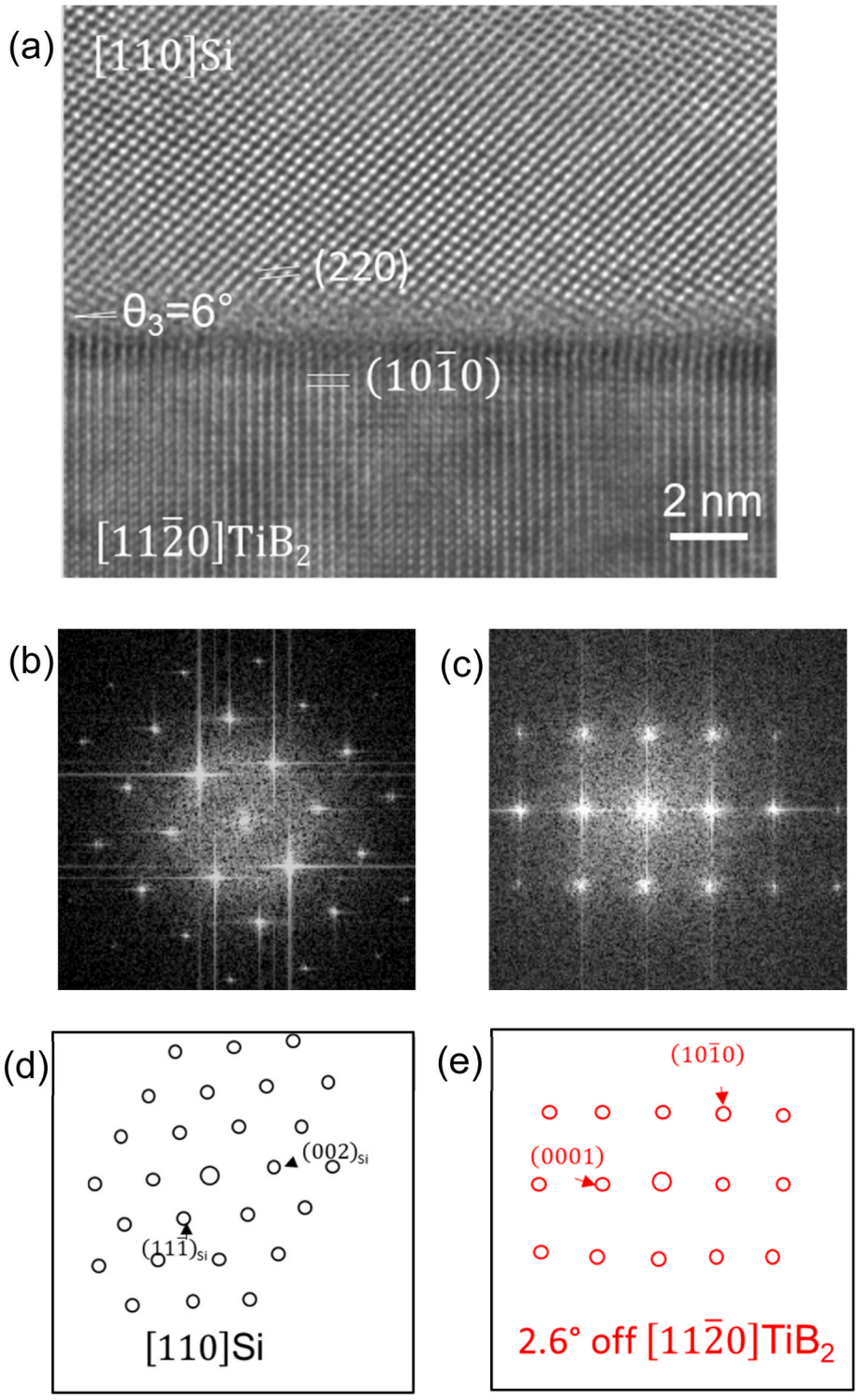

Fig. 10. (a) High resolution TEM image showing the interface between (10$\bar{1}$0) TiB_2 particle and (220) Si phase with TiB_2 and Si being viewed along [11$\bar{2}$0] (2.6° deviation) and [110], respectively; (b) and (c) are Fast Fourier transformation (FFT) patterns for TiB_2 and Si, respectively, (d) and (e) are the schematic representation of the indexed FFT patterns of (b) and (c). These results suggest the following defined orientation relationship (OR) between TiB_2 and Si: (10$\bar{1}$0) TiB_2//6° (220) Si and 2.6° [11$\bar{2}$0] TiB_2//[110]Si.

very important for the heterogenous nucleation of Si.

The ability of accommodating a wider range of impurities might also promote heterogeneous nucleation. The solubility of impurities in silicon and aluminium is different. As shown in Table 1, Fe (0.58 %), Mn (0.11 %), Ni (0.43 %) and Zn (0.33 %) are the main impurities in studied Al-27Si alloy. The silicon has lower solubility for these especially 3*d* metals such as Fe, Mn and Ni. It is reported [37] that the solubility of Fe and Mn in silicon at about 1000 °C is approximately 10^{-5} % compared to up to 0.05 wt% solubility of Fe in aluminium at the eutectic temperature [38].

Table 1
Chemical composition of the as-cast alloy (wt.%).

Alloy	Al	Si	Mg	Fe	Mn	Ti	Ni	Zn	Zr	B	SUPPLIER
CP Al	balance	<0.04	–	<0.06	–	–	–	–	–	–	Norton
Al-10Ti	Balance	0.12	0.02	0.35	–	10.7	–	–	–	–	Affilips
Al-5B	balance	0.09	–	0.17	–	–	–	–	–	5.44	Aleastur
Al-27Si	balance	27.0	–	0.58	0.11	–	0.43	0.33	–	–	This study
Al-50Si	balance	50	0.01	0.39	0.02	0.04	0.01	0.02	–	–	Avon
This master alloy	balance	1.0	0.1	1.5	0.1	3.7	0.6	0.3	0.1	1.5	This study (IPS)

Table 2
Calculated misfits of β- $Al_{4.5}FeSi$ and Si on different substrates.

Misfit *f*(%)	(0 0 0 1) TiB_2 without 2DC (along the [10$\bar{1}$0] direction of TiB_2)	(1 0 $\bar{1}$ 0) TiB_2 without 2DC (along the [0001] direction of TiB_2)	Si modified Al_3Ti 2DC at Al/(0 0 0 1) TiB_2 (along the [10$\bar{1}$0] direction of TiB_2)	Al_8Fe_5 2DC at Al/ (1 0 $\bar{1}$ 0) TiB_2 (along the [0001] direction of TiB_2)
β-$Al_{4.5}FeSi$	OR1: 9.7 %	OR2: 6.8 %	OR5: 11.09 %	***OR6: ~3 %***
Si	OR3: 13.2 %	OR4: 19 %	***OR7: 8.2 %***	OR8: −13.6 %

4.3. Composition templating for heterogeneous nucleation of Si

The interfacial segregation of Si at the Al/TiB_2 interface happened at the high temperature (800 °C) during the long holding time (4 h). The STEM-EDS mapping (Fig. 2) demonstrated the Si existing at all around surface of the TiB_2 particles, which indicates that the first layer of the Si-Si bonding has been built up. Therefore, the templating of the Si on the TiB_2 surface can potentially providing the compositional templating and enhance the heterogeneous nucleation of Si.

It has been discussed in Part 1 that Si segregation on the TiB_2 surface is due to the strong interaction between Ti and Si compare to any interaction between two elements in the melt of the Al-Ti-B-Fe-Si master alloy, which is reflected by their heat of mixing value, $\Delta H^{mix}_{Ti-Si} = -66$ kJ/mol [39]. In the segregation layer of Si, some covalent bonding among the nearby Si atoms has been built up. These pre-existing Si-Si covalent bonding in the segregation layer with low charging would help to lower the energy barriers by forming the distorted tetrahedral coordination for the Si approaching on the top.

The experimental results demonstrated that silicon phase nucleates on these modified TiB_2 particles. Two equivalent pairs of specific ORs between the primary Si and the TiB_2 particles were identified. However, the specific TiB_2 surface on which heterogeneous nucleation of silicon

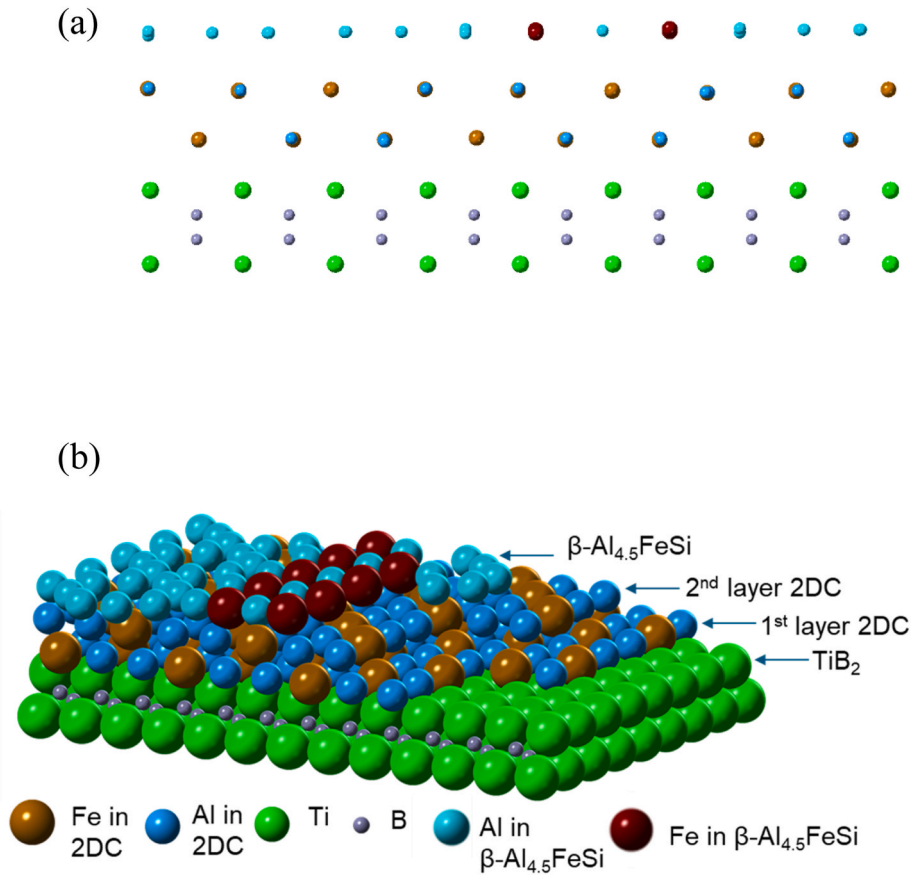

Fig. 11. Schematic illustration showing (a) the matching between the solid β-$Al_{4.5}FeSi$ on Al_8Fe_5 2DC which interfacial segregation on the TiB_2 according to the OR: ($\bar{2}$ 2 0) [1 1 0] β-$Al_{4.5}FeSi$//(0 0 1) [1 0 0] Al_8Fe_5 2DC//(1 0 $\bar{1}$ 0)[1 1 $\bar{2}$ 0] TiB_2, and (b) the 3D construction of (a), showing that the Al_8Fe_5 2DC providing the compositional templating and structural templating for the nucleation of the solid β-$Al_{4.5}FeSi$.

occurs requires further discussion. Same as above, the ORs of Si and the segregation 2DC was calculated based on the ORs between Si/TiB_2 and 2DC/TiB_2. Two new pairs of ORs (OR 7 and OR 8) are as follows based on OR 3 and OR 4:

$$(0\,0\,2)\mathrm{Si}\ //\ 5^{\circ}(1\,1\,2)\ \text{Si incorporated}\ Al_3Ti\ \text{2DC, and}\ [1\,1\,0]\mathrm{Si}\ //\ 2.6^{\circ}[\bar{2}\,0\,1]\ \text{Si incorporated}\ Al_3Ti\ \text{2DC} \quad \text{(OR 7)}$$

and

$$(2\bar{2}0)\mathrm{Si}\ //\ 6^{\circ}(0\,0\,1)Al_8Fe_5\ \text{2DC, and}\ [1\,1\,0]\mathrm{Si}\ //\ 2.6^{\circ}[1\,0\,0]Al_8Fe_5\ \text{2DC} \quad \text{(OR8)}$$

The mismatches between the solid Si and both terminated (0 0 0 1) and $(10\bar{1}0)$ planes of the modified TiB_2 particles were calculated in Table 2, compared with the values of Si matching a "clean" (no interfacial segregation) TiB_2. It is shown that nucleation of Si at the Al/(0 0 0 1)TiB_2 with and without interfacial segregation 2DC has smaller misfit than that at the Al/ $(10\bar{1}0)$ TiB_2 interface. Therefore, heterogenous nucleation more likely happens at the Al/(0 0 0 1)TiB_2 interface rather than at the Al/ $(10\bar{1}0)$ TiB_2 interface.

Additionally, the misfit between Si and TiB_2 with interfacial segregation is smaller than that with a clean surface, indicating a better structural templating. However, as it is shown that the misfit between the solid Si and the modified Al/(0 0 0 1)TiB_2 still as large as −8.2 %. Therefore, the significant refinement of Si cannot be solely attributed to improved structural templating; it also results from compositional templating caused by the interfacial segregation of Si at the Al/(0 0 0 1) TiB_2 interface.

According to the number density of the modified TiB_2 particles in the diameter range 0.2–6.0 μm in Al-3.7Ti-1.5B-1.5Fe-1.0Si master alloy, the number density of the addition TiB_2 particles in Al-27 Si alloy (5000 ppm Al-3.7Ti-1.5B-1.5Fe-1.0Si master alloy) can be estimated as 3.35×10^{11}/kg or $1.215 \times 10^{8}/m^3$. The number density of the primary Si particles in this study in Al-27Si without and with addition of 5000 ppm Al-3.7Ti-1.5B-1.5Fe-1.0Si master alloy were estimated according to the area number density as 911 and $1.49 \times 10^{6}/m^3$, respectively. The nucleation rate based on the number density of added TiB_2 and nucleated Si was calculated as 1.73 %, which is much higher than that of the β-Al4.5FeSi (0.2 %) and α-Al (maximum 1 %), indicated a very good refinement achieved.

In this work, Si is refined to an average size of 39 ± 5.5 μm, similar to that achieved by the best practice through phosphorus addition according to literature. For instance, the primary Si phase in a phosphorus-inoculated hypereutectic Al-50 Si alloy was usually coarser than 30 μm in size [25,26]. However, conventional refinement approaches such as P addition have a few disadvantages compared to inoculation by the modified TiB_2 particles. P forms unwanted intermetallic compounds with alloying elements like Mg, Fe, or Ti, and reacts antagonistically with Sr or Na whose addition for modification purpose, reducing the effectiveness of both refinement and modification. Its performance is highly sensitive to melt conditions, i.e. P can evaporate or be lost at high temperatures. Additionally, P is difficult to be removed once added and may generate toxic byproducts such as phosphine gas under certain conditions. These issues limit its consistent and safe application in industrial settings. Modified TiB_2 offers a smart refinement strategy, especially in high-Si or recycled Al-Si systems, by leveraging interfacial chemistry rather than just crystallographic matching at the interface. It provides an adaptable, and industry-relevant approach to controlling Si morphology and distribution.

4.4. Si segregation on TiB_2 interface: poisoning or promoting heterogeneous nucleation

Al-Ti-B master alloys are among the most successful and widely used grain refiner systems in aluminium industry. In recent years, studies have shown that the Al/TiB_2 interface can be significantly influenced by alloying elements present in Al alloys. One of the most well-known phenomena is the segregation of Si on the surface of TiB_2 particles, which will result in significant decrease in the refining efficiency of Al-Ti-B (with excess Ti) grain refiners, often referred to "the Si poisoning effect". This effect occurs due to the dissolution of the pre-existed Al_3Ti two-dimensional compound (2DC) at the Al/(0 0 0 1)TiB_2 interface and the subsequent formation of a two-dimensional solid solution (2DS) [40]. This transformation in structure and chemistry of the interface leads to an increase in lattice mismatch at the α-Al/TiB_2 interface, from 0.09 % at the Al_3Ti 2DC/TiB_2 interface to 4.2 % at the Al/TiB_2 interface, which is one of the major factors reducing the nucleation potency of TiB_2 for α-Al.

A positive aspect of Si interfacial segregation phenomenon is revealed in this study. Instead of inhibiting α-Al nucleation, Si segregation enhances heterogeneous nucleation of the primary Si particles in hypereutectic Al-Si alloys. As discussed in Section 4.3, Si segregation at the Al/(0 0 0 1)TiB_2 interface provides both structural and compositional templating for Si nucleation. This dual templating effect significantly enhances the heterogeneous nucleation of silicon on the surface of the Si-segregated TiB_2 particles, leading to a notable refinement of the primary Si particles.

The natural segregation of Si at the Al/(0 0 0 1)TiB_2 interface can play either a negative or positive role, depending on whether it serves as a nucleation substrate for α-Al or Si phases. The poisoning on TiB_2 by Si segregation is solely to α-Al nucleation. A deeper understanding of interfacial segregation behaviour is essential for harnessing the segregation phenomenon to optimize nucleation process. This insight would provide a valuable methodological framework for the development of highly effective grain refiners.

Structural refinement and uniformity, for example reduced size and improved distribution of Fe-rich intermetallic compounds (Fe-IMCs) and primary Si particles, are widely recognized within the aluminium community as a critical factor in promoting mechanical properties of alloys. The findings of this work, particularly the significant refinement of Fe-rich intermetallic compounds and primary Si particles, will definitely lead to notable improvements in the mechanical properties of Al alloys, as demonstrated by previous studies [41,42].

5. Summary

(1) In an Al-14.8Si-0.7Mn-3.9Fe alloy, the addition of 0.1 wt.% Al-3.7Ti-1.5B-1.5Fe-1.0Si master alloy containing in-situ synthesized TiB_2 particles with Fe and Si segregation resulted in refinement of the primary β-$Al_{4.5}FeSi$ intermetallic compound, with the average length of the primary IMC phase decreasing from 1178 ± 135 μm to 425 ± 61 μm.
(2) In a hypereutectic Al-27 Si alloy, the addition of 0.5 wt.% of the same master alloy resulted in significant refinement of the primary Si phase, with the average size decreasing from 461 ± 51 μm to 39 ± 5.5 μm.

(3) The mechanism underlying the significant refinement of the primary IMCs and primary Si is attributed to the enhanced heterogeneous nucleation of both the primary phases on the externally added TiB_2 particles where Si and Fe segregations are segregated on their surface. An orientation relationship between the primary IMC β-$Al_{4.5}FeSi$ and the TiB_2 particle, $(\bar{2}\,2\,0)$ β-$Al_{4.5}FeSi$//1.5° $(1\,0\,\bar{1}\,0)$ TiB_2, $[1\,1\,0]$ β-$Al_{4.5}FeSi$//1.5° $[1\,1\,\bar{2}\,0]$ TiB_2, is identified, providing the evidence of nucleation of the intermetallic phase on the TiB_2 surface.

(4) Heterogeneous nucleation of the primary Si phase in hypereutectic alloy is also enhanced by the added in-situ TiB_2 particles where Si segregation occurs on their surface, supported by the experimentally observed orientation relationship between the primary Si and TiB_2: $(0\,0\,0\,1)$ TiB_2//$(0\,0\,2)$ Si and $[1\,1\,\bar{2}\,0]$ TiB_2// 2.6° $[1\,1\,0]$ Si.

(5) In addition of structural templating, the compositional templating offered by the interfacial Fe and Si segregation on the TiB_2 particles plays an important role in refining the primary Fe-IMC and Si phases, demonstrating that combined structural and compositional templating offers a promising approach to enhancing heterogeneous nucleation of not only intermetallic compounds but also a single phase such as Si which is difficult to be nucleated.

CRediT authorship contribution statement

Zhongping Que: Writing – review & editing, Writing – original draft, Visualization, Validation, Methodology, Investigation, Funding acquisition, Formal analysis, Data curation, Conceptualization. **Yun Wang:** Writing – review & editing, Investigation, Data curation. **Zhongyun Fan:** Supervision, Funding acquisition, Conceptualization. **Xiaorong Zhou:** Writing – review & editing, Data curation.

Funding

This work was financial supported by the EPSRC (UK) for under grant number EP/N007638/1 (Future Liquid Metal Engineering Hub). This work is also supported by Brunel University London BRIEF award (11937131).

Declaration of competing interest

The authors declare that they have no known competing financial interests or personal relationships that could have appeared to influence the work reported in this paper.

Acknowledgement

Thanks go to LiME hub of BCAST in Brunel University London. The EPSRC is gratefully acknowledged for providing financial support under Grant EP/N007638/1. This work is also supported by Brunel University London BRIEF award (11937131). Thanks go to Dr. Changming Fang for discussion in the nucleation difficulty of single-phase Si.

Data availability

No data was used for the research described in the article.

References

[1] M.A. Easton, M. Qian, A. Prasad, D.H. StJohn, Recent advances in grain refinement of light metals and alloys, Curr. Opin. Solid State Mater. Sci. 20 (2016) 13–24.
[2] B.S. Murty, S.A. Kori, M. Chakraborty, Grain refinement of aluminium and its alloys by heterogeneous nucleation and alloying, Int. Mater. Rev. 47 (2002) 3–29.
[3] I. Maxwell, A. Hellawell, A simple model for grain refinement during solidification, Acta Metall. 23 (1975) 229.
[4] Z. Que, Y. Wang, C.L. Mendis, C.M. Fang, J. Xia, X.R. Zhou, Z. Fan, Understanding Fe-containing intermetallic compounds in Al alloys: an overview of recent advances from the LiME research hub, Metals 12 (10) (2022) 1677.
[5] D. Rabbe, et al., Making sustainable aluminium by recycling scrap: the science of "dirty" alloys, Prog. Mater. Sci. 128 (2022) 100947.
[6] D. Lu, Y. Jiang, G. Guan, R. Zhou, Z. Li, R. Zhou, Refinement of primary Si in hypereutectic Al-Si alloy by electromagnetic stirring, J. Mater. Process. Technol. 189 (1–3) (2007) 13–18.
[7] J. Jorstad, D. Apelian, Hypereutectic Al-Si Alloys: Practical Casting Considerations, 3, 2009, pp. 13–36.
[8] S.K. Das, J.A.S. Green, J.G. Kaufman, D. Emadi, M. Mahfoud, Aluminium recycling-An integrated, industrywide approach, J. Occup. Med. 62 (2) (2010) 23–26.
[9] A.M. Samuel, A. Pennors, C. Villeneuve, F.H. Samuel, H.W. Doty, S. Valtierra, Effect of cooling rate and Sr-modification on porosity and Fe-intermetallics formation in Al-6.5% Si-3.5% Cu-Fe alloys, Int. J. Cast Met. Res. 13 (4) (2000) 231–253.
[10] Z Que, Z Fan, Heterogeneous Nucleation Difficulties of Fe-Containing Intermetallic Compounds in Al Alloys, paper in preparation.
[11] Z. Que, Y. Wang, Z. Fan, T. Hashimoto, X.R. Zhou, Composition templating for heterogeneous nucleation of intermetallic compounds, Sci. Rep. 14 (1) (2024) 8968.
[12] M. Gupta, S. Ling, Microstructure and mechanical properties of hypo/hyper-eutectic Al–Si alloys synthesized using a near-net shape forming technique, J. Alloys Compd. 287 (1999) 284–294.
[13] S. Tomida, K. Nakata, S. Shibata, I. Zenkouji, S. Saji, Improvement in wear resistance of hypereutectic Al–Si cast alloy by laser surface remelting, Surf. Coat. Technol. 169–170 (2003) 468–471.
[14] K. Matsuura, M. Kudoh, H. Kinoshita, H. Takahashi, Precipitation of Si particles in a super-rapidly solidified Al–Si hypereutectic alloy, Mater. Chem. Phys. 81 (2003) 393–395.
[15] J.L. Estrada, J. Duszczyk, Characteristics of rapidly solidified aluminium–silicon–X powders for high-performance applications, J. Mater. Sci. 25 (1990) 886–904.
[16] T. Jiang, C. Yu, B. Xu, W. Yu, G. Xu, Y. Li, Z. Wang, G. Wang, A novel investigation on the influence of Cu–P modifier on the microstructure, mechanical performance, and melting process of Al–50Si alloys treated by overheating, Prog. Nat. Sci. Mater. Int. 31 (3) (2021) 461–470.
[17] S. Wang, M. Fu, X. Li, J. Wang, X. Su, Microstructure and mechanical properties of Al-Si eutectic alloy modified with Al-3P master alloy, J. Mater. Process. Technol. 255 (2018) 105–109.
[18] M. Zuo, X. Liu, H. Dai, X. Liu, Al-Si-P master alloy and its modification and refinement performance on Al-Si alloys, Rare Met. 28 (2009) 412–417.
[19] T. Gao, X. Zhu, H. Qiao, X. Liu, A new Al-Fe-P master alloy designed for application in low pressure casting and its refinement performance on primary Si in A390 alloy at low temperature, J. Alloys Compd. 607 (2014) 11–15.
[20] A.V. Pozdniakov, M.V. Glavatskikh, S.V. Makhov, V.I. Napalkov, The synthesis of novel powder master alloys for the modification of primary and eutectic silicon crystals, Mater. Lett. 128 (2014) 325–328.
[21] A.M. Samuel, E. Samuel, V. Songmene, F.H. Samuel, A comparative study of grain refining of Al-(7–17%) Si cast alloys using Al-10% Ti and Al-4% B master alloys, Materials 16 (7) (2023) 2867.
[22] G.K. Sigworth, Grain refinement of Al–Si–Cu alloys by AlB_2 and $(Al,Ti)B_2$. Tech, Commun. Now. 18 (2024) 2778–2782.
[23] Z. Que, Y. Wang, Z. Fan, et al., Interfacial segregation of Fe and Si on TiB_2 surface and refinement of Fe-bearing intermetallic compounds and primary Si, Metall. Mater. Trans. A (2025), https://doi.org/10.1007/s11661-025-07970-7.
[24] Aluminium Association, Standard Test Procedure for Aluminium Alloy Grain Refiners, TP-1, 1987. Washington DC.
[25] Y. Xu, Y. Deng, D. Casari, R.H. Mathiesen, X. Liu, Y. Li, Growth kinetics of primary Si particles in hypereutectic Al-Si alloys under the influence of P inoculation: experiments and modelling, J. Alloys Compd. 854 (2021) 155323.
[26] H.S. Dai, X.F. Liu, Refinement performance and mechanism of an Al-50Si alloy, Mater. Char. 59 (2008) 1559–1563.
[27] Z. Fan, An epitaxial model for heterogeneous nucleation on potent substrates, Metall. Mater. Trans. A 44 (2013) 1409.
[28] Z. Fan, F. Gao, B. Jiang, Z. Que, Impeding nucleation for more significant grain refinement, Sci. Rep. 10 (1) (2020) 9448.
[29] A. Hassani, K. Ranjbar, S. Sami, Microstructural evolution and intermetallic formation in Al-8wt.%Si-0.8wt.%Fe alloy due to grain refiner and modifier additions, Int. J. Miner. 19 (2012) 739–746.
[30] A.L. Geer, A.M. Bunn, A. Tronche, P.V. Evans, D.J. Bristow, Modelling of inoculation of metallic melts: application to grain refinement of aluminium by Al–Ti–B, Acta Mater. 48 (11) (2000) 2823–2835.
[31] A.S. Cooper, Precise lattice constants of germanium, aluminum, gallium arsenide, uranium, sulphur, quartz and sapphire, Acta Crystallogr. 15 (1962) 578–582.
[32] D.M. Toebbens, N. Stuesser, K. Knorr, H.M. Mayer, G. Lampert, E9: the new high-resolution neutron powder diffractometer at the berlin neutron scattering center, Mater. Sci. Forum 378 (2001) 288, 193.
[33] S.-M. Liang, R. Schmid-Fetzer, Phosphorus in Al-Si cast alloys: thermodynamic prediction of the AlP and eutectic (Si) solidification sequence validated by microstructure and nucleation undercooling data, Acta Mater. 72 (2014) 41–56.
[34] H. Jung, N. Mangelinck-Noël, C. Bergman, B. Billia, Determination of the average nucleation undercooling of primary Al-phase on refining particles from Al-5.0 wt% Ti-1.0 wt% B in Al-based alloys using DSC, J. Alloys Compd. 477 (1–2) (2009) 622–627.
[35] The Structure of Crystals, Ralph W.G. Wyckoff, 1935, Reinhold publishing corporation.

[36] L. Pauling, The nature of the chemical bond. Application of results obtained from the quantum mechanics and from a theory of paramagnetic susceptibility to the structure of molecules, J. Am. Chem. Soc. 53 (1931) 1367–1400.
[37] E.R. Weber, Transition metals in silicon, Appl. Phys. A 30 (1983) 1–22.
[38] P. Wang, H. Lu, Y. Lai, Control of silicon solidification and the impurities from an Al-Si melt, J. Cryst. Growth 390 (2014) 96–100.
[39] A. Takeuchi, A. Inoue, Classification of bulk metallic glasses by atomic size difference, heat of mixing and period of constituent elements and its application to characterization of the main alloying element, Mater. Trans. 46 (12) (2005) 2817–2829.
[40] Y. Wang, Z. Que, T. Hashimoto, X. Zhou, Z. Fan, Mechanism for Si poisoning of Al-Ti-B grain refiners in Al alloys, Metall.Mater. Trans. A 51 (11) (2020) 5743–5757.
[41] C. Liu, X. Jiao, H. Nishat, S. Akhtar, S. Wiesner, Z. Guo, S. Xiong, Characteristics of Fe-rich intermetallics compounds and their influence on the cracking behavior of a newly developed high-pressure die cast Al-4Mg-2Fe alloy, J. Alloys Compd. 854 (2021) 157121.
[42] C. Sumalatha, P.V. Chandra Sekhar Rao, V.V. Subba Rao, M.S.K. Deepak, Effect of grain refiner, modifier and graphene on the mechanical properties of hyper eutectic Al-Si alloys by experimental and numerical investigation, Mater. Today Proc. 62 (6) (2022) 3891–3900.